Development of a cathode-directed streamer discharge in air at different pressures: Experiment and comparison with direct numerical simulation

S. Pancheshnyi,* M. Nudnova, and A. Starikovskii
Moscow Institute of Physics and Technology, 9 Institutskii per., 141700 Dolgoprudnyi, Russia
(Received 19 September 2004; published 14 January 2005)

The results are given of an experimental investigation of a cathode-directed streamer discharge in synthetic air in the pressure range from 760 to 300 torr and their comparison with the results of direct numerical simulation in a 2D hydrodynamic approximation. The pattern of discharge branching upon variation of pressure is investigated experimentally. The results are given of comparison of the predicted and measured values of anode current, streamer propagation velocity, and channel diameter. It has been demonstrated that the electric field in the streamer head is hardly affected by the pressure decrease, while the electron concentration decreases with pressure by an order of magnitude. At the same time, production of chemical species in a cathode-directed streamer discharge varies at a rate of at least the second power of inverse pressure.

DOI: 10.1103/PhysRevE.71.016407 PACS number(s): 52.80.Hc

INTRODUCTION

The basic advantage of pulsed gas discharges in solving problems in plasma chemistry appears to consist of the relatively low rate of energy removal to fast-thermalized degrees of freedom of gas, which brings about a high efficiency of energy input by the channels of processes with high values of activation energy. An especially important part is played by the processes of production of chemical species (electron-excited molecules and atoms, radicals, and the like) in the discharge, which are closely associated with the dynamics of electric fields and kinetics of electrons. A detailed investigation of the elementary processes occurring in a gas discharge may both enable one to better understand the fundamental problems associated with the physics of low-temperature plasma and lead to the optimal solution of engineering problems.

At wide pressure range, the initial stage of a pulsed discharge defining the plasma characteristics occurs, as a rule, in a streamer form (see, for example, [1]). Interest in streamer discharges is explained by the need to develop a highly nonequilibrium plasma for purposes of plasma control over chemical processes (polluted gas treatment, plasma assisted combustion, surface modification, etc.) and for dealing with problems in plasma aerodynamics. Another interest shown in past years is connected to recent observations of discharges at low pressure conditions at sprite altitudes 40–90 km (see [2], and references therein).

The main objective of this study is to investigate the electrodynamic and kinetic characteristics of a cathode-directed streamer discharge at different pressures. In so doing, the experimental measurements are supplemented with numerical simulation for performing a detailed investigation of the processes occurring in the streamer channel and in its vicinity.

*Present address: Laboratoire E.M2.C, Ecole Centrale Paris, Grande Voie des Vignes, 92295 Chatenay-Malabry, France. Electronic address: pon99@mail.ru

I. EXPERIMENTAL SETUP

Figure 1 is a diagrammatic view of the experimental setup. The discharge section being evacuated is fashioned as a stainless steel cube with an edge of 220 mm. The system was evacuated by a 2NVR-5DM backing pump to a pressure of 10^{-1} torr; it could be filled with the working mixture to a maximal pressure of 2 atm. We used spectrally pure N_2:O_2 (4:1) synthetic air.

The discharge was investigated in the plane-to-plane geometry with an interelectrode gap of 30 mm. The high-voltage electrode (cathode) was made of brass in the form of a disk 80 mm in diameter, and the grounded anode was an aluminum disk 100 mm in diameter.

High-voltage pulses were transmitted from a PAKM pulse voltage generator to the high-voltage electrode of the discharge chamber via RK-50-24-13 cable with a pulse repetition rate of 0.5 to 10 Hz. The amplitude of incident pulse of negative polarity was 12 kV, with half-height duration of 22 ns with about 8 ns rise and fall times. The pulse parameters were measured using a back-current shunt placed in a break in the cable braiding such as to make possible the separation of the pulse incident from the generator from the pulse reflected from the chamber. Note that the voltage

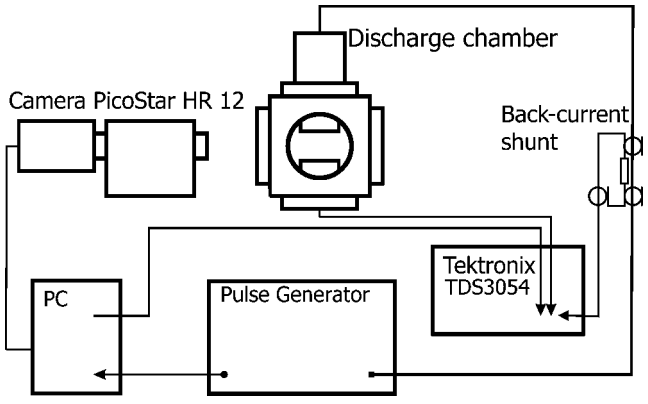

FIG. 1. Block diagram of the experimental setup.

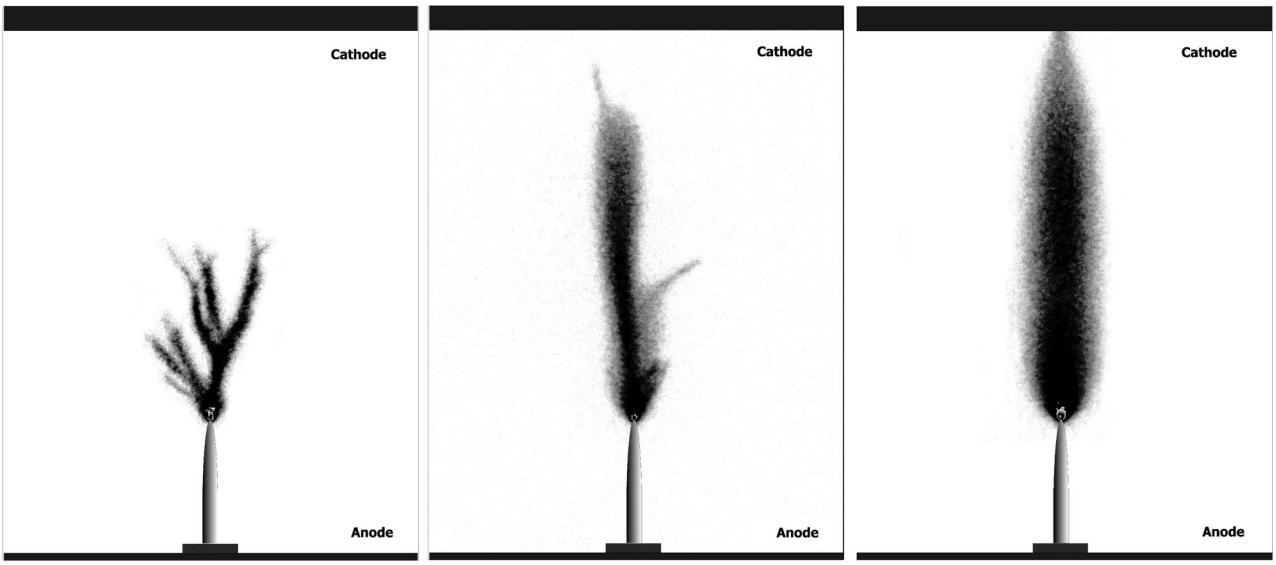

FIG. 2. Integral photographs of a streamer flash in air at pressures of 740, 500, and 380 torr.

across the high-voltage electrode is made up by the incident and reflected pulses and, because of the low discharge currents, is twice the voltage pulse in the cable.

An almost uniform electric field $E_{gap} \simeq 7$ kV/cm was realized in the interelectrode gap when high-voltage pulses were applied; in so doing, the delay time of streamer start exceeded significantly the lifetime of voltage across the gap. A steel needle 10 mm in height, 0.8 mm in diameter, and with a rounding radius of $\simeq 0.04$ mm was installed on the grounded anode for the purpose of initiating a cathode-directed streamer. When a pulse of negative polarity was delivered to the cathode, a field arose on the point of the anode needle which exceeded significantly the value of the field in the entire discharge gap. As a result, a streamer started from the anode needle. Therefore, high-voltage pulses of negative polarity were used to initiate a cathode-directed streamer developing from the grounded anode. This enabled one to directly measure the streamer flash current; for this purpose, the anode needle was placed in an open dielectric sleeve 1.5 mm in height and shunted to ground via resistors with an overall resistance of 3 Ohm. The scheme of the discharge gap and photographs of discharge development are given in Fig. 2.

A PicoStar HR12 ICCD camera by LaVision with a Helios 44M lens ($f=58$ mm, and 1:2 aperture ratio) was used to determine the space-time characteristics of the discharge. The spectral sensitivity of the system corresponds to the range from 340 to 700 nm, with the minimal exposure of 100 ps. The camera was focused via KU-1 (0.18–3.5 μm spectral range) quartz windows 100 mm in diameter and 10 mm thick onto a plane passing through the discharge chamber axis and the anode needle. The space resolution of photographs was 0.3 mm.

The camera operation was synchronized with the recording of the electrodynamic characteristics such that the photograph, the voltage across the gap, and discharge current obtained in the pulse-periodic mode of the generator operation would correspond to one and the same streamer flash. The above-identified signals were recorded by a Tektronix TDS-3054 oscilloscope; the time resolution of the system was better than 1.5 ns.

II. DIRECT NUMERICAL SIMULATION

In spite of the continuously increasing potentialities of experimental methods, the use of numerical simulation enables one to significantly improve the quality of interpretation of experimental data.

We employ a direct numerical simulation of a solitary cathode-directed streamer discharge in a two-dimensional formulation. The motion of charged particles, namely, electrons n_e and positive n_p and negative n_n ions, was described by the balance equations (1)–(3) within a hydrodynamic approximation combined with Poisson's equation (4) for the calculation of the electric field distribution in the gap,

$$\frac{\partial n_e}{\partial t} + \mathrm{div}(\vec{v}_e n_e) = S_{ion} + S_{photo} - S_{att} - S_{rec}^{ei}, \tag{1}$$

$$\frac{\partial n_p}{\partial t} = S_{ion} + S_{photo} - S_{rec}^{ei} - S_{rec}^{ii}, \tag{2}$$

$$\frac{\partial n_n}{\partial t} = S_{att} - S_{rec}^{ii}, \tag{3}$$

$$\Delta\varphi = -\frac{e}{\varepsilon_0}(n_p - n_e - n_n). \tag{4}$$

Here, φ is the electric potential, $\vec{v}_e$ is the drift velocity in the local electric field $\vec{E}$ ($\vec{E}=-\vec{\nabla}\varphi$), and S_{ion}, S_{photo}, S_{rec}^{ei}, S_{rec}^{ii}, and S_{att} are the rates of ionization, photoionization, electron-ion and ion-ion recombination, and electron attachment, respectively.

A. Plasmochemical conversion in a streamer plasma

A gas-discharge plasma usually contains many types of electronically excited atoms and molecules, simple and complex ions, etc., such factors as a relatively insignificant heating of the streamer channel and relatively low degrees of excitation, dissociation, and ionization of the gas allowed us to conclude that, on the time scales of interest to us (up to 25 ns), the discharge electrodynamics is governed primarily by the charged particles, so that we could reduce the number of processes that have to be taken into account in modeling discharges on these time scales.

We tried to simplify the complete kinetic scheme developed in [3] for N_2-O_2 mixtures to the ultimate possible extent. Charged particles of seven kinds were taken into account, namely, electrons N_2^+, O_2^+, N_4^+, O_4^+, $O_2^+N_2$, O_2^- as well as 15 reactions with their participation.

(1) Direct electron impact ionization:

$$e + N_2 \rightarrow e + e + N_2^+, \quad k_5 = f(E/N), \tag{5}$$

$$e + O_2 \rightarrow e + e + O_2^+, \quad k_6 = f(E/N). \tag{6}$$

(2) Rapid production of O_2^+ molecules in reactions involving N_2^+ molecules:

$$N_2^+ + N_2 + M \rightarrow N_4^+ + M,$$

$$k_7 = 5 \times 10^{-29}\ \mathrm{cm^6\ s^{-1}}, \tag{7}$$

$$N_4^+ + O_2 \rightarrow O_2^+ + N_2 + N_2,$$

$$k_8 = 2.5 \times 10^{-10}\ \mathrm{cm^3\ s^{-1}}, \tag{8}$$

$$N_2^+ + O_2 \rightarrow O_2^+ + N_2,$$

$$k_9 = 6 \times 10^{-11}\ \mathrm{cm^3\ s^{-1}}. \tag{9}$$

(3) Conversion of O_2^+ into O_4^+:

$$O_2^+ + N_2 + N_2 \rightarrow O_2^+N_2 + N_2,$$

$$k_{10} = 9 \times 10^{-31}\ \mathrm{cm^6\ s^{-1}}, \tag{10}$$

$$O_2^+N_2 + N_2 \rightarrow O_2^+ + N_2 + N_2,$$

$$k_{11} = 4.3 \times 10^{-10}\ \mathrm{cm^3\ s^{-1}}, \tag{11}$$

$$O_2^+N_2 + O_2 \rightarrow O_4^+ + N_2,$$

$$k_{12} = 10^{-9}\ \mathrm{cm^3\ s^{-1}}, \tag{12}$$

$$O_2^+ + O_2 + M \rightarrow O_4^+ + M,$$

$$k_{13} = 2.4 \times 10^{-30}\ \mathrm{cm^6\ s^{-1}}. \tag{13}$$

(4) Dissociative recombination:

$$e + O_4^+ \rightarrow O_2 + O_2,$$

$$k_{14} = 1.4 \times 10^{-6}(300/T_e)^{1/2}\ \mathrm{cm^3\ s^{-1}}, \tag{14}$$

$$e + O_2^+ \rightarrow O + O,$$

$$k_{15} = 2 \times 10^{-7}(300/T_e)\ \mathrm{cm^3\ s^{-1}}. \tag{15}$$

(5) Electron attachment and ion-ion recombination:

$$e + O_2 + O_2 \rightarrow O_2^- + O_2,$$

$$k_{16} = 2 \times 10^{-29}(300/T_e)\ \mathrm{cm^6\ s^{-1}}, \tag{16}$$

$$O_2^- + O_4^+ \rightarrow O_2 + O_2 + O_2,$$

$$k_{17} = 10^{-7}\ \mathrm{cm^3\ s^{-1}}, \tag{17}$$

$$O_2^- + O_4^+ + M \rightarrow O_2 + O_2 + O_2 + M,$$

$$k_{18} = 2 \times 10^{-25}\ \mathrm{cm^6\ s^{-1}}, \tag{18}$$

$$O_2^- + O_2^+ + M \rightarrow O_2 + O_2 + M,$$

$$k_{19} = 2 \times 10^{-25}\ \mathrm{cm^6\ s^{-1}}. \tag{19}$$

The rate constants $k_7 - k_{19}$ were taken from [3]. The ionization rate constants $k_5 - k_6$, the electron drift velocity v_e, and the effective electron temperature T_e were calculated by solving the Boltzmann kinetic equation in the two-term approximation with the help of the BOLSIG software package [4]. In three-body reactions above the letter M represents molecules N_2 and O_2.

Thus it is possible to rewrite right part terms of the balance equations (1)–(3) in the following form: $S_{ion} = k_5[N_2]n_e + k_6[O_2]n_e$; $S_{att} = k_{16}[O_2][O_2]n_e$; $S_{rec}^{ei} = k_{14}[O_4^+]n_e + k_{15}[O_2^+]n_e$; $S_{rec}^{ii} = k_{17}[O_2^-][O_4^+] + k_{18}[O_2^-][O_4^+][M] + k_{19}[O_2^-][O_2^+][M]$; while charged particles densities in the form $n_p = [N_2^+] + [N_4^+] + [O_2^+] + [O_4^+] + [O_2^+N_2]$; and $n_n = [O_2^-]$. Here the density of heavy particles is denoted by square brackets. It is assumed that density of neutral particles are not changed during the task, while the density of each type of ions was recalculated with the help of reactions (5)–(19) at every time step.

One can conclude from the schema above that the charge exchange and conversion of ions $N_2^+ \rightarrow O_2^+ \rightarrow N_4^+$ occur on a time scale of several nanoseconds (see, for example, [5]). Therefore, it is necessary to keep in mind that the main charged particles in "cold" air plasma at high pressures are electrons, positive O_4^+ ions, and negative O_2^- ions [6].

B. Initial distribution of charged particles and streamer onset

It was assumed that the heavy particles (neutral molecules and molecular ions) were stationary throughout the entire period of streamer charge development. At the initial instant of time, the gas in the gap was assumed to be fully quasineutral and, in order to initiate the formation of a streamer channel, preionization was preassigned,

$$n_e(z,r)|_{t=0} = n_i(z,r)|_{t=0} = n_0 \exp\left[-\left(\frac{z}{\sigma_z}\right)^2 - \left(\frac{r}{\sigma_r}\right)^2\right], \quad (20)$$

where $n_0 = 10^{14}$ cm^{-3}, $\sigma_z = 0.1$ mm, and $\sigma_r = 0.05$ mm.

Note that this model is almost completely self-consistent and contains no "fitting" parameters except for the initial level of preionization which is of critical importance to the start of the streamer. By way of reducing the level of initial preionization to $n_0|_{\min} = 10^5$ cm^{-3}, it was found that this parameter has a significant effect on the start delay time and almost no effect on the streamer characteristics when removed to a distance of $z^*/\sigma_z \simeq (4-5) < 0.5$ mm from the electrode tip [5,7]. The preionization parameters employed by us correspond in fact to the streamer start without a delay. However, as will be demonstrated below, in view of the fairly short time of voltage rise, this condition agrees well with the measurement results.

C. Photoionization processes

The rate of gas photoionization, S_{photo}, is described in the same manner as in [7] and based on the model [8]:

$$S_{photo} = \frac{1}{4\pi}\frac{p_q}{p+p_q}\int_V d^3\vec{r}_1 \frac{S_{ion}(\vec{r}_1)}{|\vec{r}-\vec{r}_1|^2}\Psi(|\vec{r}-\vec{r}_1|p), \quad (21)$$

where $1/4\pi$ is the normalizing constant, p is the gas pressure, p_q is the quenching pressure for the photoionizing states, and $\Psi(|\vec{r}-\vec{r}_1|p)$ is the coefficient of absorption of the ionizing radiation in the medium. Identification of the emitted and ionizing states can be found, for example, in [2].

In spite of the relatively small length of the gap, the process of electron emission from the cathode under the effect of radiation from the streamer head was disregarded. The photoemission is the determining process in simulating the collision of a cathode-directed streamer with a surface at distances corresponding to the path of short-wave radiation. Proceeding from the radiation spectrum of N_2-O_2 mixtures in nanosecond discharges and from the photoelectric work function in the case of brass (over 4 eV), the distances for which the photoemission from the cathode must be taken into account amount to fractions of a millimeter at atmospheric pressure. This result is in good agreement with experiment, where almost no cathode radiation is observed down to the lowest pressures.

D. Computational mesh

High spatial gradients of the particle density and electric field impose limits on the computational cell size. It was found that for every pressure and voltage (or rather, streamer diameter) there is a maximum size of a cell near the streamer head and increase of this value leads to significant (10% or more) deviation of the main streamer parameters. For this reason a numerical grid with spatial steps up to 3×10^{-3} mm (for atmospheric pressure) and up to 3×10^{-2} mm (for 300 torr pressure case) always covered the region of intense ionization and preionization in front of the streamer head. Out of the detailed part of the mesh the space step increased exponentially as the boundary of the calculation region was approached.

The total number of mesh cells in the radial direction was kept to be constant as 192, whereas in the axial direction, it varied from 256 at the initial instant, to about 750 as the peak of the electric field moved along the discharge gap.

The time step, which is determined by the electron transport processes at the electric field maximum, was, as a rule, in the range of $(1-5)\times10^{-13}$ s, which is significantly smaller than that required for stability of the used numerical scheme.

III. BASIC RESULTS

A. Spatial development of a streamer flash

Some time (start delay time) after a high voltage is applied to the discharge gap, a streamer flash starts which is accompanied by the propagation of the radiation front. Note that an ionization wave always developed from the anode needle point toward the cathode; the development of a weak opposite ionization wave was observed only under conditions of low pressure when the cathode-directed streamer approached the cathode to a distance of the order of the streamer head radius. Typical integral photographs of a streamer flash, obtained with an exposure of about 50 ns for pressures of 740, 500, and 380 torr, are given in Fig. 2.

It follows from these results that the region of intense radiation increases significantly with decreasing pressure: the streamer channel becomes both longer and wider. As a result of an increase in the channel length, a spark discharge could develop in the gap during the time of a high-voltage pulse with the pressure decreased to 320 torr.

At pressures above 320 torr, the measurement results (Fig. 2) demonstrate two different forms of discharge development, namely, at a pressure of 740 torr the discharge is a branching structure with a set of simultaneously developing channels, while at a pressure of 380 torr a single channel is observed. As a result of our investigations, three pressure ranges may be identified.

Only a branching streamer flash is observed at pressures above 680 torr; in so doing, the number of channels varies from two to five. The number of branchings decreases with pressure, because no more than three streamer channels are formed at pressures of 650 to 620 torr.

In the medium-pressure range from 590 to 500 torr, both a branching structure and a single channel are recorded in different runs. This range is transient from the standpoint of the emergence of branching of the streamer channel.

Only a single streamer channel is observed at pressures below 470 torr.

As was mentioned previously, when the pressure was decreased to 320 torr, the discharge had enough time to change to the spark form. When the interelectrode gap was increased to 50 mm, the working pressure range could be extended to 80 torr, which also corresponded to the instant of transition of the discharge to the spark form. Due to the long streamer onset time, the maximal pressure for this gap was limited to 410 torr, and only a single channel was observed for all pressures used.

Therefore, one can conclude that the probability of branching of the streamer channel varies significantly with pressure and, under our experimental conditions, results in branching only at pressures above 470 torr. A further increase in pressure causes an increase in the number of branchings per unit length.

The results obtained here are in good qualitative agreement with the results recently presented in [9], where formation of positive streamers in a 17 mm gap in air for maximum voltages 21 kV was studied at pressures from 760 to 75 torr. It was observed that at high pressure the discharge has more and thinner streamers than at low pressure. At 760 torr, their number also increases with voltage while at lower pressures their number remains constant, i.e. four streamers at 300 torr, two at 150 torr, and one at 75 torr.

Note that the flash registered in the experiment is due both to the branching of streamer channels in the volume and to a simultaneous start of several streamers in high spatially nonuniform electric fields in the vicinity of the anode needle point. Under our experimental conditions, the branching of the discharge in the majority of cases was due to the development of several channels from the anode; along with this, however, modes with branching of channels in the gap were observed (Fig. 2).

B. A criterion of streamer branching

A comparison of the measured frequencies of streamer branching with a theory is labored. The theoretical treatment of this process is extremely hampered due to the lack of clear knowledge of the branching mechanism, and there are only a few papers dealing with this problem.

Recently, authors of [2] assumed, that the maximum diameter of the expanding streamers is predominantly controlled by the combination of the absorption cross section $\chi_{\min}=3.5\times10^{-3}$ mm^{-1} torr^{-1} of the molecular oxygen (O_2) at 102.5 nm and the partial pressure of molecular oxygen, P_{O_2}. At this, streamers exhibit branching when their diameter becomes greater than D_{cr},

$$D_{cr}=\frac{2k_+}{\chi_{\min}P_{O_2}}, \tag{22}$$

where k_+ is a dimensionless parameter. This parameter is expected to be different for positive and negative streamers.

At this work, the diameter was measured by the base of the radiation profile at midlength of the streamer channel, and the results are given in Fig. 3 for all pressure range (see Sec. III F for details). By using the criterion proposed, as contrasted to results of theoretical prediction [2], we found that a streamer exhibit branching when its diameter becomes *smaller* than D_{cr}. At that, the dimensionless parameter was selected to be $k_+\simeq(0.20\pm0.05)$ for the best approximation of our results (Fig. 3).

It is a well known fact, that a planar front of ionization wave is unstable and exhibits a tendency to bifurcation (see, for example [10]). A photoionization process, that produces seed electrons before the streamer head, is the only process that stabilizes an ionization front. This stabilization effect allows a streamer channel to branch only when the streamer diameter is less than D_{cr}. For the same reason, a streamer becomes more stable at high voltages and/or low pressures.

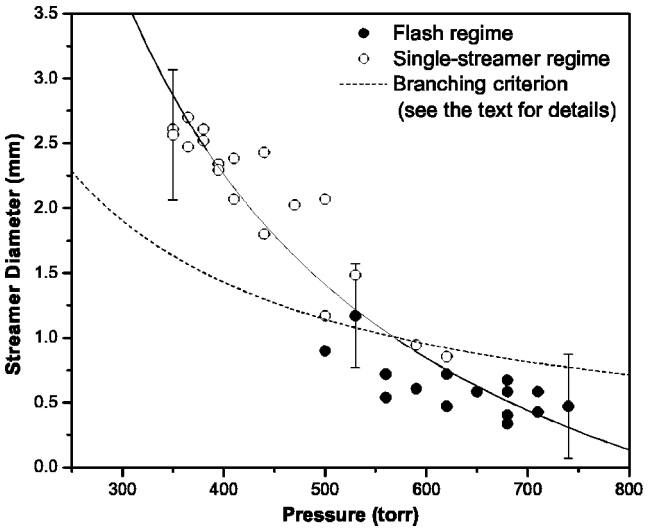

FIG. 3. Measured diameter of the streamer channel at different pressures for multichannel (flash) and single-channel regimes. A comparison with the criterion of branching (22).

C. Streamer flash current

In determining the discharge current, one must take into account the gap charging current that flows through the anode. The capacitive displacement current was determined experimentally and found to agree well with the calculated value. The capacitance of the needle-plane system was 1.7×10^{-2} pF.

Figure 4 gives the peak values of the streamer flash current at different pressures. The measurement results demonstrate that the amplitude value of the streamer current increases significantly with decreasing pressure—from

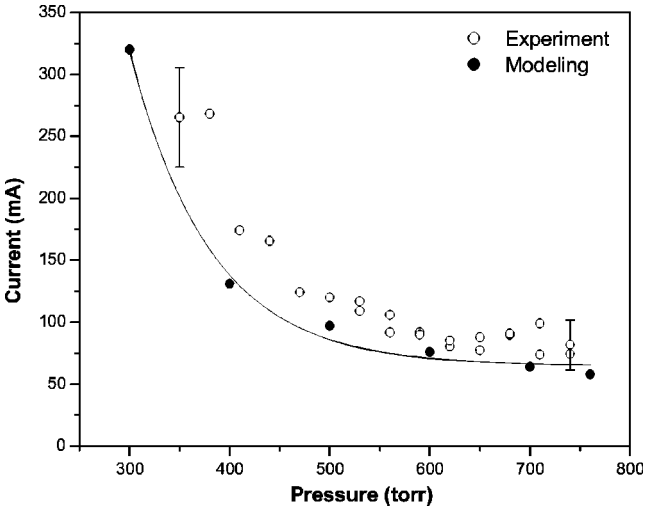

FIG. 4. The peak value of the streamer conduction current at different pressures. The results of measurements and their comparison with the results of direct numerical simulation.

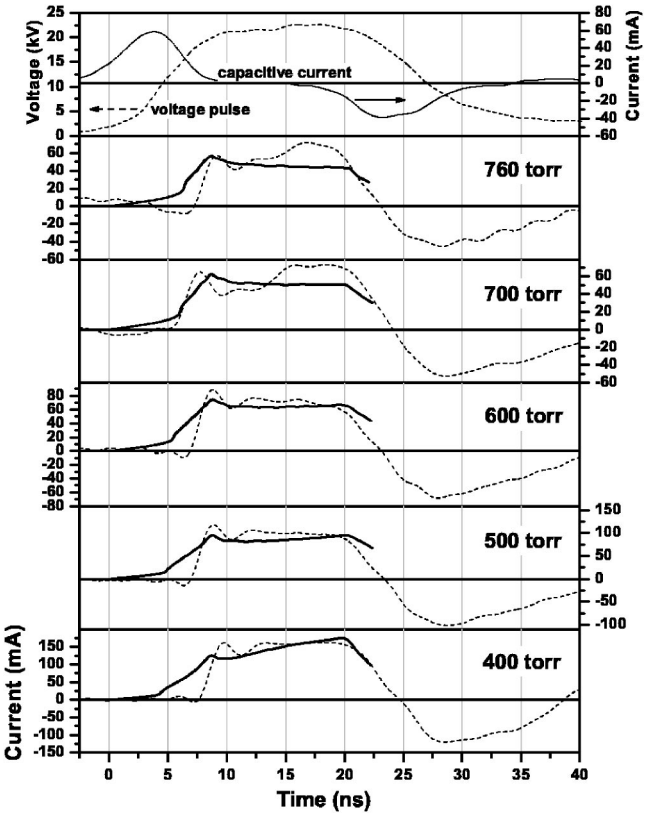

FIG. 5. Comparison of the values of the streamer conduction current at different pressures: calculated profiles (continuous curves) and measurement results (broken curves). The top graph gives the shapes of voltage across the anode and the calculated capacitive current.

70–80 mA at atmospheric pressure to 250–300 mA at a pressure of 350 torr.

A more detailed comparison is made in Fig. 5 which gives the time profiles of the streamer conduction current at different pressures. Also given for comparison is a high-voltage pulse and capacitive displacement current for the gap.

Note that the delay time of streamer start at each value of pressure may amount to a significant fraction of the high-voltage pulse duration; because the conditions of instantaneous start given by Eq. (20) are preassigned in simulation, Fig. 5 gives only experimentally obtained profiles with short times of start delay. One can see in the figure that the calculated shape of the current curve is in adequate agreement with the measured one.

D. Propagation velocity

The streamer propagation velocity was determined by the recorded position of the streamer head at different instants of time corresponding to a single flash.

For this purpose, we used the ICCD camera in the stroboscope mode with modulation of the camera amplifier using an rf signal from a G5-78 generator. Under our conditions, we used square pulses with a duration of 1.26 ns and repetition rate $f_{gate}=5.0\ \mathrm{ns}^{-1}$; in so doing, the CCD matrix was in the signal accumulation mode with the exposure time significantly exceeding the high-voltage pulse duration (about 5 ms). Examples of such photographs are given in Fig. 6 for three values of pressure.

This approach enables one to record the positions of the streamer head with the frequency f_{gate} and determine the value of velocity at different instants of time. The propagation velocity was determined as the product of the repetition rate f_{gate} of control pulses by the recorded distance between instantaneous images of the streamer head. The values of the propagation velocity in different cross sections of the discharge gap are given in Fig. 7 for pressures of 700, 500, and 400 torr.

One can see that, under similar conditions, the behavior of discharge development varies with decreasing pressure. For example, the streamer motion at high and medium pressures

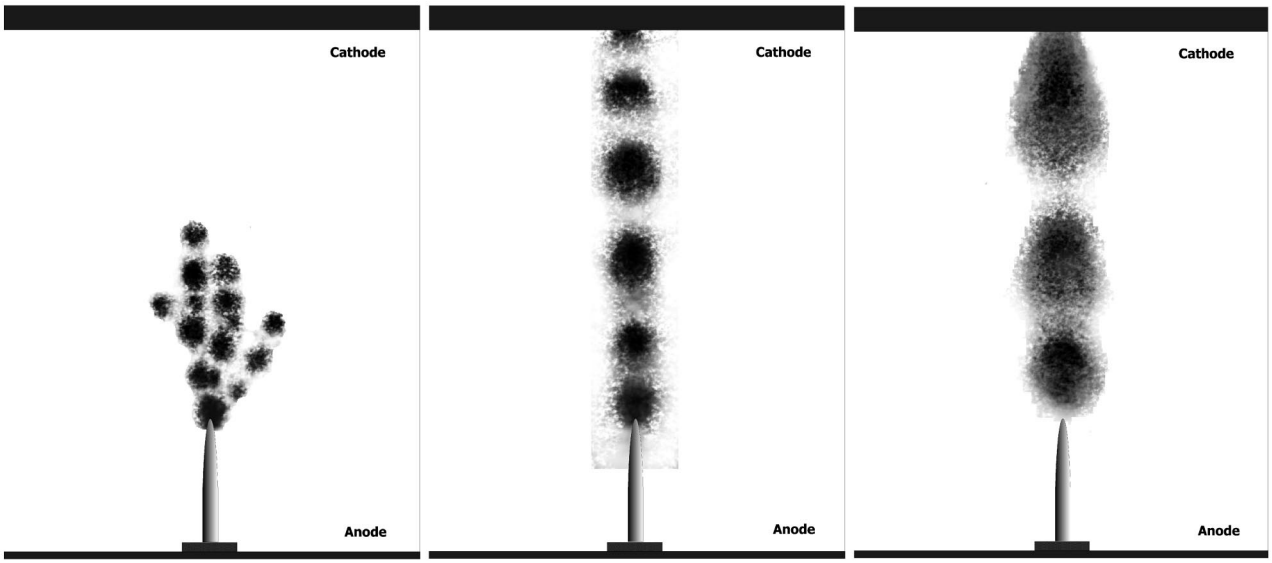

FIG. 6. Time-resolved photographs of a streamer flash in air at pressures of 740, 500, and 380 torr. A stroboscopic mode with a repetition rate of 5.0 ns^{-1} and exposure duration of 1.26 ns.

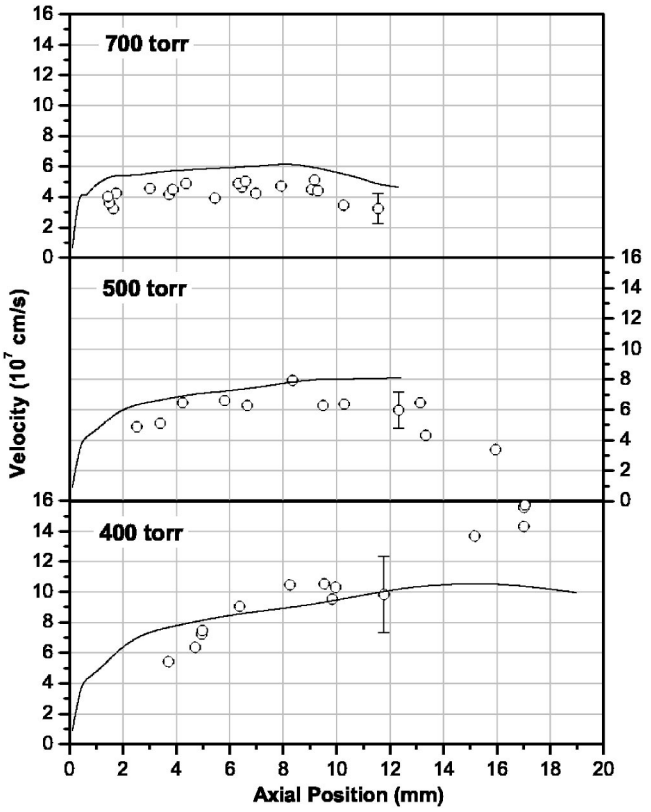

FIG. 7. Comparison of the values of the front propagation velocity at different pressures: calculated profiles (continuous curves) and experimental points.

is almost uniform throughout the high-voltage pulse duration; it is only over times corresponding to the trailing edge of the voltage pulse that the discharge deceleration and stopping is observed. At low pressures close to the threshold of spark discharge generation, a continuous acceleration of the discharge is observed.

The values of the gap average velocity for different pressures are given in Fig. 8. The measurement results indicate that the streamer velocity increases significantly with decreasing pressure—from 4×10^7 cm/s at atmospheric pressure to 1.5×10^8 cm/s at a pressure of 350 torr.

The values of the rate of discharge development obtained during numerical simulation are given in Figs. 7 and 8 for comparison.

E. Correlation between the radiative and electrodynamic characteristics of discharge

From the standpoint of more detailed analysis and comparison of the experimentally recorded radiation profiles with the results of numerical simulation, it must be emphasized that the determining contribution to the radiation spectrum of an N_2-O_2 mixture acted upon by a nanosecond discharge in the visible and ultraviolet spectral region is made by the radiation of the 2^+ system of nitrogen corresponding to $N_2(C\,^3\Pi_u \rightarrow B\,^3\Pi_g)$ transition (see, for example, [11]). In view of the low degree of excitation of gas, the experimentally recorded radiation I at point $\vec{r}$ at the instant of time t is

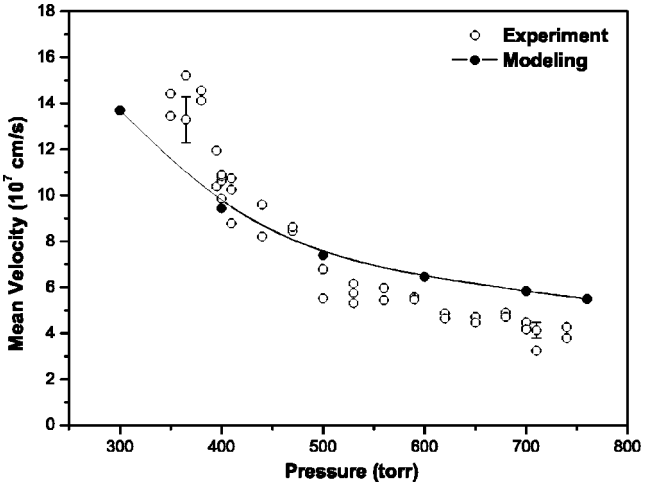

FIG. 8. The gap average velocity of streamer propagation for different pressures. The measurement results and their comparison with the results of direct numerical simulation.

proportional to the $N^*(\vec{r},t)$ concentration of radiating state of $N_2(C\,^3\Pi_u)$ at the given point.

The concentration of electronically excited state of nitrogen molecules is defined by the processes of direct electronic excitation (23), spontaneous radiation (24), and collision quenching (25) and (26),

$$N_2(X\,^1\Sigma_g^+) + e \xrightarrow{k_{ex}} N_2(C\,^3\Pi_u), \tag{23}$$

$$N_2(C\,^3\Pi_u) \xrightarrow{1/\tau_0} N_2(B\,^3\Pi_g) + h\nu, \tag{24}$$

$$N_2(C\,^3\Pi_u) + N_2 \xrightarrow{k_q^{N_2}} \text{products}, \tag{25}$$

$$N_2(C\,^3\Pi_u) + O_2 \xrightarrow{k_q^{O_2}} \text{products}. \tag{26}$$

Here, k_{ex} is the rate constant of electronic excitation of the $N_2(C\,^3\Pi_u)$ level from the ground state; $\tau_0=42$ ns is the radiative lifetime; and $k_q^{N_2}=0.13\times10^{-10}$ cm^3/s and $k_q^{O_2}=3.0\times10^{-10}$ cm^3/s are the quenching rate constants on the N_2 and O_2 molecules, respectively. The dependence of the rate constant of electronic excitation on the reduced electric field $k_{ex}(E/N)$ was calculated using the BOLSIG software package [4], and the lifetime and the quenching rate constants were borrowed from [12].

The concentration of $N_2(C\,^3\Pi_u)$ at every instant of time may be determined in accordance with the kinetic equation

$$\frac{dN^*(\vec{r},t)}{dt} = k_{ex}(\vec{r},t)n_e(\vec{r},t)[N_2] - \frac{N^*(\vec{r},t)}{\tau}. \tag{27}$$

Here, τ is the overall lifetime of radiating state, defined by the processes (24)–(26),

$$\frac{1}{\tau} = \frac{1}{\tau_0} + k_q^{N_2}[N_2] + k_q^{O_2}[O_2]. \tag{28}$$

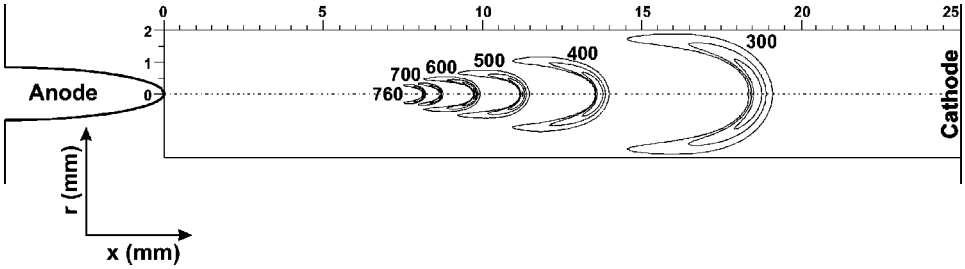

FIG. 9. Instantaneous distribution of the excitation rate of the $N_2(C\,^3\Pi_u)$ state by direct electron impact from the ground state (23) for pressures of 760, 700, 600, 500, 400, and 300 torr at the instant of time of 21 ns. The isolines correspond to the values of 10^{20}, 10^{21}, 10^{22}, and 10^{23} cm^{-3}/s. Results of direct numerical simulation.

In dry air, the lifetime of the $N_2(C\,^3\Pi_u)$ state varies from 0.6 ns at atmospheric pressure to 1.2 ns at a pressure of 350 torr.

The excitation rate $k_{ex}n_e$ was determined from direct numerical simulation. Figure 9 gives the calculated instantaneous distribution of the excitation rate for several values of pressure at the instant of time of 21 ns. It follows from the graph that a pressure decrease is accompanied by an increase in the streamer velocity and in the region of gas excitation.

The concentration of the electronically excited state of $N_2(C\,^3\Pi_u)$ at an arbitrary instant of time T may be determined from Eq. (27) in the form

$$N^*(\vec{r},T) = [N_2]\int_0^T k_{ex}(\vec{r},t)n_e(\vec{r},t)\exp\left(-\frac{T-t}{\tau}\right)dt. \quad (29)$$

Figure 10 gives the instantaneous distribution of radiation ($I \sim N^*$) at the instant of time $T_0=20$ ns at a pressure of 500 torr. It follows from the figure that the excitation of gas occurs in a narrow region in the streamer head, while the afterglow of gas is observed in the streamer channel region over distances of the order of the product of the streamer velocity (Fig. 8) by the lifetime of the radiating states (28).

In comparing the simulation results with experiment, one must project a three-dimensional axisymmetric object from the space $\vec{r}=(x,r)$ onto the observation plane (x,y) where the x direction coincides with the discharge axis. This transformation (direct Abel's transformation) follows from the fact that the experimentally recorded $\Phi(x,y,T)$ radiation is integrated over the y chords in each cross section,

$$\Phi(x,y,T_0) \sim \int_{-\infty}^{\infty} N^*(x,r,T_0)dl, \quad (30)$$

where $r^2=y^2+l^2$.

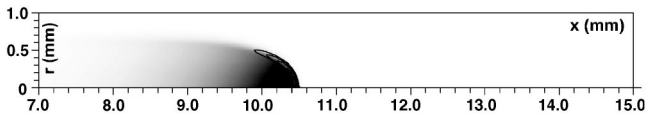

FIG. 10. The isolines of 5, 10, 25, 50, and 100% of the instantaneous rate of excitation of radiation and the image of instantaneous spatial distribution of radiation $[I(\vec{r},T_0)]$ at the instant of time $T_0=20$ ns. The pressure is 500 torr.

Relations (29) and (30) connect calculated dynamics of electric field and electron density and measured streamer emission for a time moment T_0. However, experimentally measured emission Φ_Σ is not instantaneous, but integrated during time gate T_{gate},

$$\Phi_\Sigma(x,y,T_0,T_{gate}) = \int_0^{T_{gate}} \Phi(x,y,T_0+t)dt. \quad (31)$$

The calculated Φ_Σ images at a pressure of 500 torr at the instant of time $T_0=20$ ns for the accumulation time $T_{gate}=0.1$, 1.0, and 5.0 ns are given in Fig. 11. The discharge propagation velocity under these conditions amounted to 8.3×10^7 cm/s. From symmetry considerations, only halves of the image are given in the figure.

F. Channel diameter

As it was mentioned above, the diameter was measured by the base of the radiation profile at midlength of the streamer channel, and the results are given in Fig. 12 for the investigated pressure range. It follows from the graph that the dependence of the streamer channel diameter D on the inverse pressure $1/P$ may be represented as

$$D = A\left(\frac{1}{P}-\frac{1}{P_0}\right), \quad (32)$$

and gives the following values of the approximation parameters for the measured dependence: $A=1.7\times10^3$ mm torr

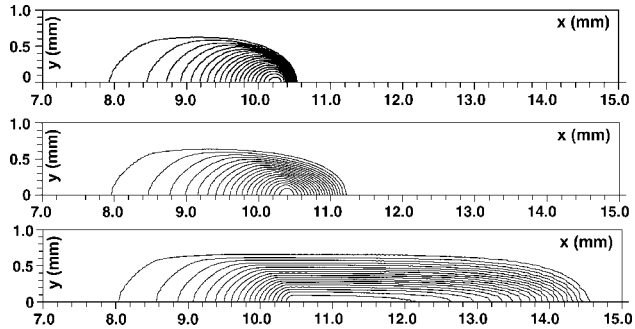

FIG. 11. Isolines of the image projection $[\Phi_\Sigma(x,y,T_0,T_{gate})]$ with a step of 5% of the amplitude at the instant of time $T_0=20$ ns with the accumulation time $T_{gate}=0.1$, 1.0, and 5.0. The pressure is 500 torr.

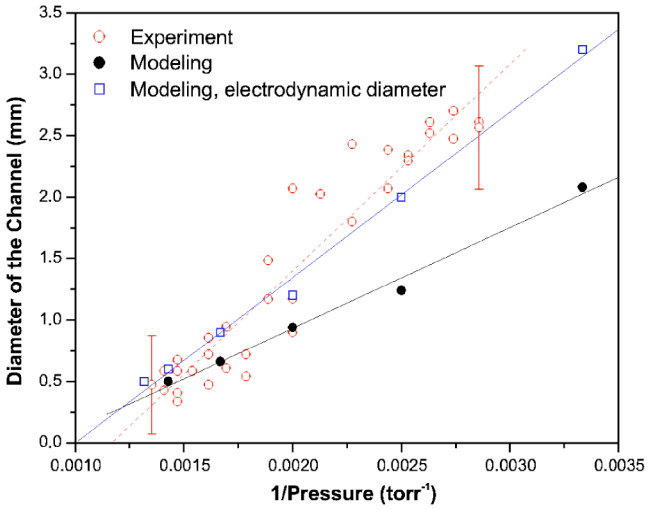

FIG. 12. The streamer channel diameter, determined by the half-height of the radiation profile, as a function of inverse pressure. Measurement results and results of direct numerical simulation.

and $P_0=855\pm30$ torr. Therefore, the channel diameter decreases to zero with increasing pressure, i.e., the pressure P_0 is the limiting pressure at which a streamer channel may exist in dry air at a voltage $U_{\max}\simeq 22\pm2$ kV. Under a higher pressure for a not very small discharge gap, streamer head cannot propagate and space charge will diffuse and recombine, the current will go to zero and the discharge extinguishes.

This criterion does not correspond to an existence of stability field of 5 kV/cm at atmospheric pressure (about 20 Td of reduced electric field) [13]. It was shown, that a streamer can exist in a regime of deceleration even for lower values of electric field (see, for example, [14]). Streamer stagnation is accompanied by a monotonic decrease in the radius of the streamer head and an increase in the maximum electric field in the head.

Note that several methods may be employed to determine the streamer channel diameter by the results of numerical simulation. Because the streamer channel is bounded by a narrow region of uncompensated charge with very steep boundaries [5], it is this particular, *electrodynamic*, channel diameter that is most frequently referred to in one way or another as the streamer diameter when performing simulation [15]. Nevertheless, for direct comparison with experiment, it is necessary to calculate the *radiative* channel diameter (29)–(31).

Also given in Fig. 12 is the streamer channel diameter determined by both methods for different pressures. Comparison reveals that the measured and calculated values of the radiative diameter of the channel differ by a factor of approximately two in the greater part of the investigated range.

We have not yet managed to find the reason for such discrepancy between the calculated and measured values of the channel diameter. On the one hand, the underestimation of the calculated radiative diameter may be associated with disregard of the cascade processes in determining the rate of excitation of the $N_2(C\,^3\Pi_u)$ state. On the other hand, the tendency toward self-excitation of the microchannel plate of the camera intensifier may bring about a decrease in the space resolution of photographs during measurements with short exposure times of the intensifier of the ICCD camera. The latter assumption is favored by the fact that a channel diameter of 0.15–0.20 mm is usually observed for similar parameters of the discharge in air at atmospheric pressure [16], which is approximately a half of the value obtained by us and fits adequately the results of direct numerical simulation.

Note that better agreement between the calculated and measured values of the electrodynamic diameter (Fig. 12) is accidental and should not be regarded as an accuracy criterion of simulation. However, it is worthy of note that the pressure dependence of the streamer channel diameter for all three sets of points is well approximated by relation (32) which was predicted previously on the basis of an analytical model of streamer discharge development [7,17].

G. The efficiency of using a streamer discharge in plasma-chemical processes at different pressures

Plasma-chemical transformations of atoms and molecules over short times are largely associated with electron kinetics which, in turn, are closely associated with the electrodynamics of the discharge, i.e., are almost completely defined by the electric field and electron density in plasma. In [11], an example of species with formation thresholds of 5.42 [NO(A)], 11.2 [N_2(C)], and 18.6 eV [N_2^+(B)] is used to demonstrate that chemical species are produced mainly in the streamer head, i.e., in the region of high electric fields. In so doing, no appreciable production of electron-excited components in the streamer channel could be observed at any values of the interelectrode gap, including the mode of partial closure of the discharge gap by the streamer up to the realization of sparkover.

Figure 13 gives the axial profiles of the electron concentration and electric field at the instant of time of 21 ns for different pressures; it follows from the figure that the E/N electric field is hardly affected by the pressure decrease, while the n_e electron concentration decreases with pressure by an order of magnitude.

In view of this, one could assume a significant decrease in the efficiency of production of species in streamer plasma as a result of decreasing pressure.

In addition, when the pressure decreases, the channel diameter (Fig. 12) increases at a faster rate than the anode discharge current (Fig. 4), so that the calculated density of streamer current decreases monotonically from 30 A/cm^2 at atmospheric pressure to 5 A/cm^2 at a pressure of 300 torr. On the other hand, it follows from Fig. 14, which gives the relative radiative characteristics of streamer flash in the entire gap during the entire time of discharge development, that the overall production of the $N_2(C\,^3\Pi_u)$ electron-excited state increases significantly with decreasing pressure.

In spite of the fact that the rate of quenching of electron-excited states varies almost linearly with pressure (28), this effect is largely a result of the increase in the characteristic dimensions, namely, the channel diameter and front thick-

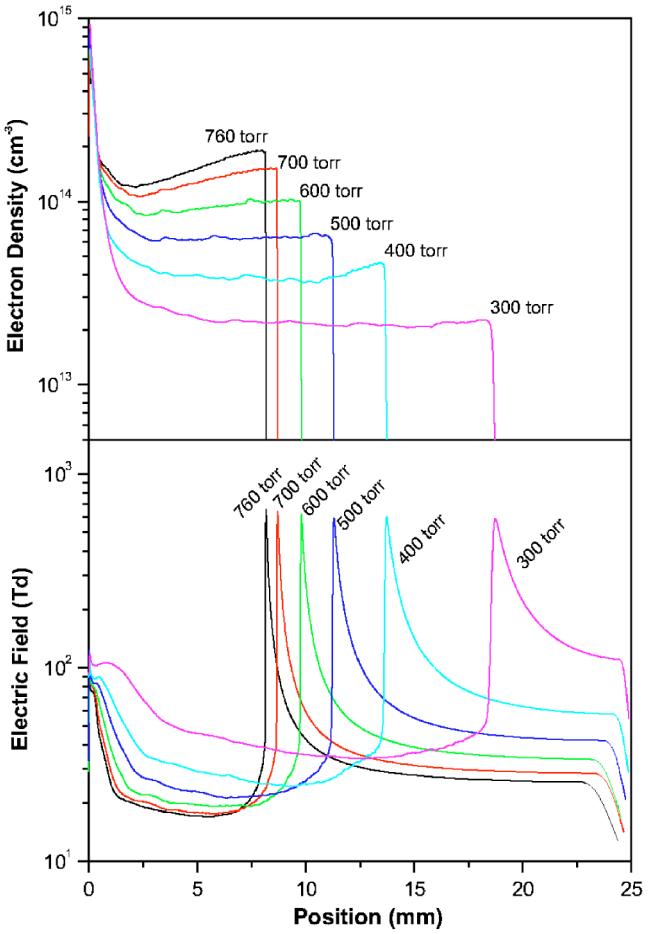

FIG. 13. Profiles of electron concentration and reduced electric field on the discharge axis at the instant of time of 21 ns for pressures of 760, 700, 600, 500, 400, and 300 torr. Results of direct numerical simulation.

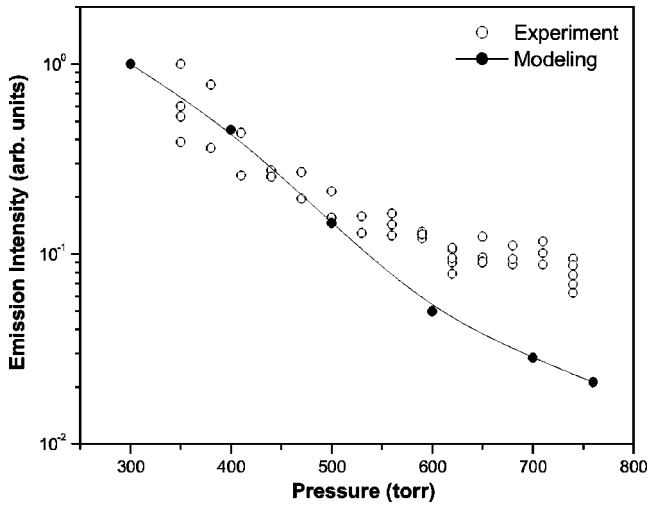

FIG. 14. Relative value of integral radiation of streamer discharge as a function of pressure. Measurement results and their comparison with results of direct numerical simulation.

ness, with decreasing pressure. For example, when the pressure decreases from 760 to 300 torr, the width of the region of intensive production of $N_2(C\,^3\Pi_u)$ increases by approximately an order of magnitude (Fig. 9).

Therefore, it may be inferred that the density of production of highly excited particles in the streamer discharge plasma hardly varies with pressure. In so doing, in view of the fact that the streamer channel diameter increases linearly with decreasing pressure (32), the overall production of chemical species per streamer channel increases as at least the second power of inverse pressure.

More detailed analysis of the results of numerical simulation reveals that, at high pressures, the streamer discharge stops; this is accompanied by a significant increase in the electron concentration and electric field in the head [14]. Nevertheless, because of an abrupt decrease in the streamer head radius, no increase is observed in the total production of species.

Based on simple similarity scaling lows, authors of [2] predicted that the streamer timescales, the streamer spatial scales, and the streamer electron densities scale with the air density N as $\sim 1/N$, $\sim 1/N$, and $\sim N^2$, respectively, and the scaled streamer characteristics remain otherwise identical for the same values of the reduced electric field E/N. However, an experimental study performed in [9] shows that streamer flash structure is not simply determined by reduced electric field. The results of the present work are also in a partial contradiction with results of the model [2]. Indeed, for example, the reduced electric field in the streamer channel is proportional to reverse gas pressure, while the reduced electric field in the streamer head is approximately constant over all pressures.

These deviations of the theory and experimental results arise due to the important role of photoionization processes in cathode-directed streamer propagation. Development of streamer discharge is mainly governed by processes in the streamer head. An analysis made in [7,17] demonstrates that production of photoelectrons by ionizing radiation from the head plays no less a role in the formation of the positive streamer head than the following gain of the avalanche under the effect of collisional ionization in the electric field of the streamer head. In such a way, the linearity of the system (1)–(4), that describes dynamics of ionization wave propagation, is failed due to highly nonlinear photoionization term (21). Strongly coupled chemical kinetics in the streamer plasma also leads to rejection of similarity scaling lows.

However, sometimes, particularly in a case of nonwave structure of the discharge, the similarity scaling lows well describe the experimental results. For example, a good agreement was shown for a quasiuniform streamer-to-spark transition in a short gap [18].

IV. COMPARISON OF MEASUREMENT RESULTS WITH RESULTS OF THE SIMULATION

First of all, note that, because of the failure to take into account the processes of electron emission from the electrode surfaces, the employed numerical model cannot adequately describe the discharge in the case of decreasing voltage across the gap, in particular, at the trailing edge of the pulse. Indeed, when the anode potential decreases, the streamer

channel potential remains virtually constant and, at a certain instant of time, begins to exceed the anode potential; this causes the reversal of the direction of current flow. The change of sign of current is indeed observed experimentally at the trailing edge of high-voltage pulse (Fig. 5). Therefore, in spite of the fact that the anode remains the anode for the environment when the voltage at the trailing edge of the pulse decreases, the anode acquires a negative potential relative to the streamer channel, i.e., it must effectively emit electrons for the neutralization of the streamer charge. Proceeding from this restriction, the results of numerical simulation with the voltage pulse employed by us have no physical meaning over times longer than 21 ns.

Another fact to be taken into account consists in that this model provides for the development of a single channel, whereas experimentally a group of streamers is observed at high pressures (Fig. 2). The foregoing results of comparison of the calculated and measured values of anode current, propagation velocity, and streamer channel diameter demonstrate adequate agreement. Differences in the high-pressure region, where numerical simulation predicts a 30–35% higher streamer development rate, are due to the presence of simultaneously developing streamer channels which partly screen one another [19]: this is not included in the model.

Upon transition to lower pressures, numerical simulation predicts underestimated characteristics of the streamer. This difference is apparently associated with a more complex process of photoionization of gas than is assumed by us in accordance with [8].

Note that the calculated value of anode current is in better agreement with the measured value than the values of the remaining characteristics; this is indicative of its weak sensitivity to the dynamics of discharge development.

CONCLUSIONS

We have presented the results of experimental investigation of a cathode-directed streamer discharge in synthetic air in the pressure range from 760 to 300 torr and their comparison with the results of direct numerical simulation in a 2D hydrodynamic approximation.

It has been demonstrated that the pattern of discharge branching varies significantly with pressure. Under our experimental conditions, a highly branching flash is recorded at high pressures (over 680 torr), a branching structure and a single channel are recorded at medium pressures (500 to 900 torr), and only a single streamer channel always develops at lower pressures (below 470 torr). A criterion of streamer branching [2] has been checked, and principal corrections were proposed.

The results of comparison of calculated and measured values of the anode current and of the velocity of discharge propagation have demonstrated their agreement within 30–35%.

The results of investigations have shown that the streamer channel diameter varies proportionally to inverse pressure (32). For the voltage 22 ± 2 kV, the quantity 855 ± 30 torr is the limiting pressure at which a streamer discharge may form for any pulse duration for plane-to-plane discharge gap configuration.

It follows from the results that the electric field is hardly affected by the pressure decrease, while the electron concentration decreases with pressure by an order of magnitude. It has been demonstrated that the production of chemical species in a cathode-directed streamer discharge varies at a rate of at least the second power of inverse pressure.

ACKNOWLEDGMENTS

This study was conducted within the framework of a grant by the President of Russian Federation for Young Scientists and Scientific Schools (MK-313.2003.02) and was supported in part by the Ministry of Education of Russian Federation (Project No. E02-3.2-98) and by the US Civilian Research and Development Foundation (Project Nos. RP1-5002-MO-03 and PR0-1439-MO-02).

[1] Y. P. Raizer, *Gas Discharge Physics* (Springer-Verlag, Berlin, 1991).
[2] N. Liu and V. P. Pasko, J. Geophys. Res., [Atmos.] **109**, A04301 (2004).
[3] I. A. Kossyi, A. Yu. Kostinsky, A. A. Matveyev, and V. P. Silakov, Plasma Sources Sci. Technol. **1**, 207 (1992).
[4] CPAT & Kinema Software, http://www.siglo-kinema.com/bolsig.htm
[5] S. V. Pancheshnyi and A. Yu. Starikovskii, J. Phys. D **36**, 2683 (2003).
[6] N. L. Aleksandrov and E. M. Bazelyan, J. Phys. D **8**, 285 (1999).
[7] S. V. Pancheshnyi, S. M. Starikovskaia, and A. Yu. Starikovskii, J. Phys. D **34**, 105 (2001).
[8] M. B. Zheleznyak, A. Kh. Mnatsakanyan, and S. V. Sizykh, Teplofiz. Vys. Temp. **20**, 423 (1982).
[9] T. M. P. Briels, E. M. van Veldhuizen, and U. Ebert (unpublished).
[10] C. Montijn, B. Meulenbroek, U. Ebert, and W. Hundsdorfer, Phys. Rev. E **69**, 036214 (2004).
[11] S. V. Pancheshnyi, S. V. Sobakin, S. M. Starikovskaia, and A. Yu. Starikovskii, Plasma Phys. Rep. **26**, 1054 (2000).
[12] S. V. Pancheshnyi, S. M. Starikovskaia, and A. Yu. Starikovskii, Chem. Phys. **262**, 349 (2000).
[13] E. M. van Veldhuizen and W. R. Rutgers, J. Phys. D **35**, 2169 (2002).
[14] S. V. Pancheshnyi and A. Yu. Starikovskii, Plasma Sources Sci. Technol. **13**, B1 (2004).
[15] N. Yu. Babaeva and G. V. Naidis, J. Phys. D **29**, 2423 (1996).

[16] E. M. van Veldhuizen, P. C. M. Kemps, and W. R. Rutgers, IEEE Trans. Plasma Sci. **30**, 162 (2002).
[17] M. M. Nudnova, S. V. Pancheshnyi, and A. Yu. Starikovskii, in 42nd AIAA Aerospace Sciences Meeting and Exhibit, Reno, Nevada, AIAA paper 0353, 2004 (unpublished).
[18] S. Achat, Y. Telsseyre, and E. Marode, J. Phys. D **25**, 661 (1992).
[19] G. V. Naidis, J. Phys. D **29**, 779 (1996).